Acta Crystallographica Section B
Structural Science, Crystal Engineering and Materials
ISSN 2052-5206

Competition between hydrogen and halogen bonding in the structures of 5,10-dihydroxy-5,10-dihydroboranthrenes

Krzysztof Durka, Sergiusz Luliński, Katarzyna N. Jarzembska, Jaromir Smętek, Janusz Serwatowski and Krzysztof Woźniak

Acta Cryst. (2014). B**70**, 157–171

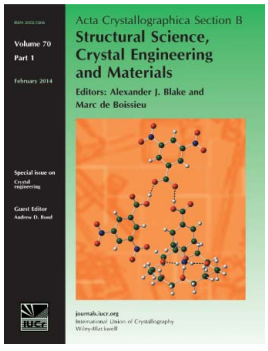

Acta Crystallographica Section B: Structural Science, Crystal Engineering and Materials publishes scientific articles related to the structural science of compounds and materials in the widest sense. Knowledge of the arrangements of atoms, including their temporal variations and dependencies on temperature and pressure, is often the key to understanding physical and chemical phenomena and is crucial for the design of new materials and supramolecular devices. *Acta Crystallographica B* is the forum for the publication of such contributions. Scientific developments based on experimental studies as well as those based on theoretical approaches, including crystal-structure prediction, structure–property relations and the use of databases of crystal structures, are published.

Acta Crystallographica Section B
Structural Science, Crystal Engineering and Materials
ISSN 2052-5206

Competition between hydrogen and halogen bonding in the structures of 5,10-dihydroxy-5,10-dihydroboranthrenes

Krzysztof Durka,[a]* Sergiusz Luliński,[a] Katarzyna N. Jarzembska,[b] Jaromir Smętek,[a] Janusz Serwatowski[a] and Krzysztof Woźniak[b]*

[a]Department of Chemistry, Warsaw University of Technology, Noakowskiego 3, Warszawa 00-664, Poland, and [b]Department of Chemistry, University of Warsaw, Pasteura 1, Warszawa 02-093, Poland

Correspondence e-mail: kdurka@gmail.com, kwozniak@chem.uw.edu.pl

Received 7 August 2013
Accepted 30 December 2013

X-ray crystallographic and computational studies are reported for a series of boranthrenes, substituted with halogen atoms. The role of competitive hydrogen (O—H···O, O—H···F, C—H···O) and halogen (Cl···Cl, O···Br, F···F) bonding interactions on the molecular arrangement in the crystal structures is discussed. The structural analysis and calculations reveal that the O—H···O hydrogen bond in the unsubstituted derivative 5,10-dihydroxy-5,10-dihydroboranthrene, $C_{12}H_{10}B_2O_2$, is of moderate strength (*ca* −20 kJ mol^{-1}), but weaker than that in the related thiophene derivative 4,8-dihydro-4,8-dihydroxy-*p*-diborino[2,3-*b*:5,6-*b*]dithiophene, $C_8H_6B_2O_2S_2$ (*ca* −40 kJ mol^{-1}). This is due to shielding of the OH group by the H atoms in the β-position of the boranthrene unit. Structural diversity derived from the flexibility of the O—H···O hydrogen bond facilitates the occurrence of other competitive interactions. For instance, in the 1,6-difluoro derivative, $C_{12}H_8B_2F_2O_2$, the crystal packing results from O—H···F and F···F interactions. In turn, the 1,6-dibromo derivative, $C_{12}H_8B_2Br_2O_2$, is dominated by Br···O halogen-bond interactions. In the most interesting case, the 1,6-dichloro derivative, $C_{12}H_8B_2Cl_2O_2$, molecular disorder leads to the formation of two different supramolecular arrangements co-existing in the crystal lattice, one based on the Cl···Cl and C—H···O bonds, and the other stabilized by O—H···O hydrogen bonds. Calculations performed with density-functional theory (DFT; *CRYSTAL09*) and *PIXEL* methodologies show that both lattices are characterized by similar energy values (*ca* −100 kJ mol^{-1}). A mixed arrangement with random or short-range-ordered molecular orientations can also be expected.

1. Introduction

Non-covalent interactions play a very important role in crystal engineering, supramolecular chemistry, biology and medicine. Strong and directional hydrogen bonds are used to control the formation of supramolecular entities and to produce networks with desired structural features and physicochemical properties (Jeffrey, 1997; Gilli & Gilli, 2009; Grabowski, 2006). Apart from hydrogen bonding, halogen-bond interactions such as $D\cdots X—A$ (X = F, Cl, Br, I; D = F, Cl, Br, I, N, O, S) are also utilized in many supramolecular strategies. Intermolecular contacts with covalently bonded halogen atoms result in weak but highly directional interactions governing packing motifs in supramolecular assemblies in the solid state (Hassel, 1970; Nayak *et al.*, 2011; Ramasubbu *et al.*, 1986). Recent experiments and theoretical calculations have shown that the electron density around a halogen atom is not spherical, but its distribution is anisotropic. Regions of charge concentration

are found in the plane perpendicular to the C—*X* bond, whereas charge depletion (termed σ-hole) occurs along the C—*X* axis (Awwadi *et al.*, 2006; Bui *et al.*, 2009; Dikundwar & Row, 2012; Hathwar, Thakur *et al.*, 2011; Hathwar & Row, 2011; Metrangolo & Resnati, 2012).

O—H···O hydrogen bonds play a major role in controlling self-assembly processes and, in general, they dominate over halogen-derived interactions. Theoretical and experimental investigations confirm that the total stabilization energy of a halogen-bond interaction is in most cases less than the strength of typical O—H···O interactions (Metrangolo & Resnati, 2008*a*). Nevertheless, recent examples show that a competition between hydrogen and halogen bonding occurs in some cases (Aakeröy *et al.*, 2007; Cimino *et al.*, 2007; Corradi *et al.*, 2000; De Moliner *et al.*, 2003; Metrangolo & Resnati, 2008*b*; Mugnaini *et al.*, 2006; Priimagi *et al.*, 2012). For instance, theoretical and experimental studies on nitroxide radicals ($R_2NO^{\bullet}$) have demonstrated that they behave as strong electron donors in halogen bonding with alkyl and benzyl halides (Cimino *et al.*, 2007; Mugnaini *et al.*, 2006). The strength of such interactions is close to that of strong hydrogen bonds with corresponding aliphatic alcohols and phenols. Crystallization of 1,2-bis(4-pyridyl)ethane from a solution containing equimolar amounts of hydroquinone (a hydrogen-bond donor) and 1,4-diiodotetrafluorobenzene (a halogen-bond donor) led to the formation of 1,4-diiodotetrafluorobenzene/1,2-bis(4-pyridyl)ethane co-crystals, while the hydroquinone remains in solution (Corradi *et al.*, 2000). Aakeröy *et al.* investigated co-crystals of 2-(pyridin-4-yl)-1*H*-benzimidazole and 4-halo-2,3,5,6-tetrafluoroaldoximes (hal = F, Br, I), where halogen and hydrogen bonds can co-exist in the same crystal structure (Aakeröy *et al.*, 2007). Complexes of poly(4-vinylpyridine) with azobenzene dyes constitute another example (Priimagi *et al.*, 2012). The competitive effects of both types of interactions are also observed in biological systems. For instance, the Holliday junction, which is an intermediate formed during homologous recombination of DNA, is stabilized through the O···Br interaction, whereas the hydrogen-bonded isomer is not formed (Metrangolo & Resnati, 2008*b*). Examples of short halogen contacts, which co-exist with hydrogen-bond interactions, have also been found in ligand–protein complexes (De Moliner *et al.*, 2003).

In recent years, the dihydroboranthrenes, which in terms of topology are close analogues of anthracene, have received much attention due to their applications in catalysis and functional materials construction. For instance, 5,10-dimethyl-5,10-dihydroboranthrene has been used as a bidentate Lewis acid for the activation of 1,2-diazines in the inverse-electron-demand Diels–Alder reaction (Kessler *et al.*, 2011; Kessler & Wegner, 2010). Moreover, the ability of B atoms to incorporate into extended π-electron systems has been exploited for the development of conductive polymers and in organic light-emitting diodes (OLEDs; Chai *et al.*, 2009; Januszewski *et al.*, 2011; Kessler *et al.*, 2011). The use of perfluoro-5,10-dichloro- and 5,10-di(pentafluorophenyl)-5,10-dihydroboranthrene as co-catalysts in olefin polymerization has also been reported (Metz *et al.*, 2000). In addition, the analogous derivatives with the 6,13-diborapentacene ring system have been applied as *n*-type organic semiconductors (Chen *et al.*, 2008).

As part of our interest in organoboron supramolecular chemistry, we have focused our attention on the structures of 1,6-dihalogenated-5,10-dihydroxy-5,10-dihydroboranthrenes. In this work, we demonstrate that the self-assembly of these compounds can be based on two types of interactions, *i.e.* hydrogen and/or halogen bonding, which may be either competitive or cooperative. In order to contrast directly the hydrogen and halogen bond, we have compared the crystal structures of four derivatives, namely: 5,10-dihydroxy-5,10-dihydroboranthrene (I) and its 1,6-dihalogenated analogues [*X* = F, Cl, Br for (II), (III) and (IV), respectively]. In addition, to elucidate the influence of molecular geometry on the crystal packing, we have analysed the structure of 4,8-dihydro-4,8-dihydroxy-*p*-diborino[2,3-*b*:5,6-*b*]dithiophene (V). The strength of the halogen- and hydrogen-bond interactions is crucial for the assembly process. In the extreme case, it leads to molecular disorder, and, furthermore, to the formation of two distinct supramolecular arrangements, either based on the halogen bonds or the hydrogen bonds. Thus, the aim of this study is to understand the role of particular intermolecular contacts present in the investigated systems. The crystallographic study is complemented by theoretical calculations which further enlighten the differences between hydrogen- and halogen-bonded systems. The cohesive energy calculations are performed using the programs *CRYSTAL09* (Dovesi *et al.*, 2005, 2009) and *PIXEL* (Gavezzotti, 2002, 2003*a*,*b*). In addition, the *PIXEL* methodology allows for calculation of dimer interaction energies (E_D^P), which were further compared with the values obtained using a supermolecular method within *GAUSSIAN09* (Frisch *et al.*, 2009), and to the energies based on charge-density distribution topology derived from the Espinosa–Lecomte estimation (Abramov, 1997; Espinosa *et al.*, 1998, 1999).

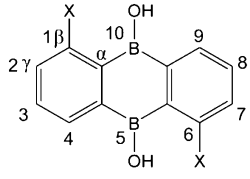

(I) X = H
(II) X = F
(III) X = Cl
(IV) X = Br

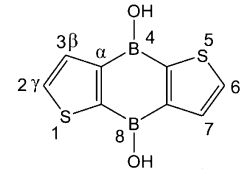

(V)

2. Experimental

2.1. Materials

All compounds were obtained according to previously reported procedures (Borowska *et al.*, 2012; Luliński *et al.*, 2013). Single crystals of (I)–(V) were grown by slow evaporation of acetone solutions.

Table 1
Experimental details.

Experiments were carried out at 100 K with Mo $K\alpha$ radiation. H-atom parameters were constrained.

	(I)	(II)	(III)
Crystal data			
Chemical formula	$C_{12}H_{10}B_2O_2$	$C_{12}H_8B_2F_2O_2$	$C_{12}H_8B_2Cl_2O_2$
M_r	207.82	243.80	276.70
Crystal system, space group	Orthorhombic, $P2_12_12_1$	Monoclinic, $P2_1/c$	Monoclinic, $P2_1/n$
a, b, c (Å)	4.8645 (4), 13.0540 (11), 15.5080 (14)	17.909 (6), 3.7790 (1), 17.355 (3)	7.3645 (10), 3.8696 (6), 20.125 (3)
β (°)	90	117.51 (4)	97.543 (14)
V (Å^3)	984.78 (15)	1041.7 (5)	568.55 (15)
Z	4	4	2
μ (mm^{-1})	0.09	0.12	0.56
Crystal size (mm)	0.10 × 0.07 × 0.06	0.11 × 0.10 × 0.07	0.15 × 0.14 × 0.13
Data collection			
Diffractometer	KUMA KM4 CCD	KUMA KM4 CCD	KUMA KM4 CCD
Absorption correction	Multi-scan *CrysAlis PRO* (Agilent, 2011)	Multi-scan *CrysAlis PRO* (Agilent, 2011)	Multi-scan *CrysAlis PRO* (Agilent, 2011)
T_{min}, T_{max}	0.428, 1.000	0.995, 1.000	0.421, 1.000
No. of measured, independent and observed [$I > 2\sigma(I)$] reflections	10 703, 2096, 1474	45 182, 4294, 3245	8905, 1906, 977
R_{int}	0.079	0.041	0.109
(sin $\theta/\lambda)_{max}$ (Å^{-1})	0.633	0.798	0.750
Refinement			
$R[F^2 > 2\sigma(F^2)]$, $wR(F^2)$, S	0.081, 0.220, 1.05	0.043, 0.124, 1.03	0.064, 0.165, 0.99
No. of reflections	2096	4294	1906
No. of parameters	145	163	164
No. of restraints	0	0	12
H-atom treatment	H-atom parameters constrained	H-atom parameters constrained	H-atom parameters constrained
$\Delta\rho_{max}$, $\Delta\rho_{min}$ (e Å^{-3})	1.01, −0.36	0.46, −0.26	0.27, −0.30

	(IV)	(V)†
Crystal data		
Chemical formula	$C_{12}H_8B_2Br_2O_2$	$C_8H_6B_2O_2S_2$
M_r	365.62	219.87
Crystal system, space group	Monoclinic, $P2_1/n$	Trigonal, $R\overline{3}$
a, b, c (Å)	8.988 (3), 3.9050 (8), 16.841 (5)	24.719 (2), 24.719 (2), 4.6681 (4)
α, β, γ (°)	90, 96.11 (3), 90	90, 90, 120
V (Å^3)	587.7 (3)	2470.2 (5)
Z	2	9
μ (mm^{-1})	6.88	0.45
Crystal size (mm)	0.13 × 0.11 × 0.09	0.20 × 0.03 × 0.03
Data collection		
Diffractometer	KUMA KM4 CCD	Bruker Kappa *APEX*-II Ultra
Absorption correction	Multi-scan *CrysAlis PRO* (Agilent, 2011)	Multi-scan *SORTAV* (Blessing, 1995, 1997)
T_{min}, T_{max}	0.428, 1.000	0.529, 1.000
No. of measured, independent and observed [$I > 2\sigma(I)$] reflections	8654, 1402, 1195	13 594, 1158, 1061
R_{int}	0.083	0.051
(sin $\theta/\lambda)_{max}$ (Å^{-1})	0.673	0.632
Refinement		
$R[F^2 > 2\sigma(F^2)]$, $wR(F^2)$, S	0.041, 0.107, 1.06	0.053, 0.193, 1.29
No. of reflections	1402	1158
No. of parameters	82	93
No. of restraints	0	27
$\Delta\rho_{max}$, $\Delta\rho_{min}$ (e Å^{-3})	1.29, −1.37	1.09, −0.35

Computer programs: *CrysAlis PRO* (Agilent, 2011), *APEX2*, *CrysAlis PRO*, *SAINT* (Bruker, 2011), *SAINT*, *SHELXS2013* (Sheldrick, 2008). † Disordered solvent molecules were incorporated in the model using *PLATON*/*SQUEEZE* (Spek, 2009). The chemical formula and formula mass correspond only to (V).

2.2. Crystal structure determinations

Single crystals of (I)–(IV) were measured on a Kuma KM4 CCD κ-axis diffractometer with graphite-monochromated Mo $K\alpha$ radiation, while measurement of (V) was performed on a Bruker Kappa APEX II Ultra diffractometer with TXS rotating anode (Mo $K\alpha$ radiation). All non-H atoms were refined anisotropically. All H atoms were visible in difference-Fourier maps, but were placed in idealized positions and refined as riding.

A crystal structure of (I) has been published previously (CSD: IBUSIJ; Januszewski *et al.*, 2011), but the data were measured at 165 K and no detailed discussion of the crystal structure was given. Hence, we repeated the measurement at 100 K, and we found another polymorphic form. The structural features of both polymorphs of (I) are briefly discussed in the text. Our structure of (I) is of moderate quality due to the fact that the compound crystallized as tiny needles, and a high-resolution cut-off of 0.75 Å was applied. In the case of (III), the molecule is disordered in two orientations around an inversion centre, with refined site occupancy factors 0.620 (3):0.380 (3). The atoms of the two components are located very close to each other, thus resulting in extensive overlap of the corresponding electron density contributions. Nevertheless, both molecules could be refined independently and only atoms C5*A* and C5*B* were restrained so that their displacement parameters approximate isotropic behaviour (ISOR in *SHELXL*). In the case of (V) the thiophene groups were also found to be disordered, and modeled in two orientations with refined site occupancy factors 0.815 (9):0.185 (9). The disordered C atoms were refined using ISOR restraints. As the contribution of the second component is small, restraints were also applied to ensure a reasonable geometry for the thiophene groups. The structure of (V) possesses open channels running along the *c* axis, which are partially occupied by solvent molecules. The included guest molecules were found to be highly disordered and their positions could not be determined. Thus, the *SQUEEZE* option of the *PLATON* program (van der Sluis & Spek, 1990; Spek, 2009) was used to eliminate the contribution of the guest molecules. Selected crystallographic data are summarized in Table 1, and difference Fourier maps generated for all of the compounds (using *MAPVIEW* in *WinGX*; Farrugia, 2012) are included in the supporting information.[1]

2.3. Computational methods

2.3.1. *CRYSTAL09* calculations. To provide more reliable geometries for further computational investigations, atomic coordinates of all the studied compounds were optimized with constrained unit-cell parameters using the *CRYSTAL09* program (Dovesi *et al.*, 2005, 2009). Calculations were performed at the DFT(B3LYP) (Becke, 1988; Lee *et al.*, 1988; Perdew, 1986) level of theory, with the 6-31G(d,p) molecular (Krishnan *et al.*, 1980) all-electron basis set found to be sufficient for the purpose of this study (Durka *et al.*, 2012; Jarzembska *et al.*, 2012; Maschio *et al.*, 2011). Both Grimme dispersion correction (Grimme, 2004, 2006) and correction for the basis set superposition error were applied (Boys & Bernardi, 1970). Ghost atoms were selected up to a 5 Å distance from the studied molecule in a crystal lattice, and were used for the basis-set superposition error estimation. The evaluation of Coulomb and exchange series was controlled by five thresholds, set to values of 10^{-7}, 10^{-7}, 10^{-7}, 10^{-7} and 10^{-25}. The condition for the SCF convergence was set to 10^{-7} on the energy difference between two subsequent cycles, while the shrinking factor was equal to 8. The cohesive energy values ($E_{\rm coh}^{\rm C}$) were calculated following the literature procedure (Civalleri *et al.*, 2008). According to expectations, the differences in molecular geometries between the optimized and non-optimized (with X—H distances elongated) structures are especially noticeable for the H-atom positions of the OH groups. The positions of the non-H atoms remained fairly unchanged during the optimization.

2.3.2. Single-point calculations. Dimer interaction energies ($E_{\rm D}^{\rm G}$) were evaluated using the *GAUSSIAN09* program package (Frisch *et al.*, 2009) using geometries taken from the *CRYSTAL09* calculations. Grimme's B97D functional was used (Grimme, 2004, 2006), which includes dispersion, together with augmented correlation-consistent polarized triple-zeta Dunning's basis set (aug-cc-pVTZ; Dunning, 1989). The obtained $E_{\rm D}^{\rm G}$ values were corrected for basis-set superposition error using the counterpoise procedure.

In order to provide a deeper examination into the intermolecular relations within the studied structures, we have prepared topological analyses of the calculated electron densities (B97D/aug-cc-pVTZ) of selected crystal dimers with their geometry taken from the optimized structures. This methodology has been successfully applied in previous studies of hydrogen- and halogen-bonded systems (Blanco *et al.*, 2009; Eskandari & Zariny, 2010; Jarzembska *et al.*, 2012; Jarzembska, Kamiński *et al.*, 2013; Lu *et al.*, 2007; Xu *et al.*, 2009). According to the topological analysis of the electron density distribution within the quantum theory of atoms in molecules (QTAIM; Bader, 1990; Matta & Boyd, 2007; Popelier, 2000), the electron density at the (3,−1) critical point, $\rho(r_{\rm BCP})$, can be used to describe the strength of a bond. Furthermore, recent investigations on hydrogen-bonded systems have shown that charge-density distribution features can be linked with the energy of a hydrogen bond. In the Espinosa–Lecomte approach (Abramov, 1997; Espinosa *et al.*, 1998, 1999), the weak interaction energy ($E_{\rm top}^{\rm G}$) of a particular intermolecular interaction is considered to be equal to approximately half of the estimated potential energy density value at the critical point, $V(r_{\rm CP})$. The formula linking the charge density topological features with the electronic energy density at a given point is given by the following equations

$$E_{\rm top}^{\rm G} = \frac{1}{2}V\left(r_{\rm CP}\right) \tag{1}$$

$$V\left(r_{\rm CP}\right) = \frac{\bar{h}^2}{4m}\nabla^2\rho(r_{\rm CP}) - 2G(r_{\rm CP}) \tag{2}$$

$$G\left(r_{\rm CP}\right) = \left(\frac{3}{10}\right)(3\pi)^{2/3}\rho^{5/3}\left(r_{\rm CP}\right) + \frac{1}{72}\frac{||\nabla\rho\left(r_{\rm CP}\right)||^2}{\rho\left(r_{\rm CP}\right)} + \left(\frac{1}{6}\right)\nabla^2\rho\left(r_{\rm CP}\right), \tag{3}$$

where $\rho\left(r_{\rm CP}\right)$ is the electron density, $\nabla^2\rho(r_{\rm CP})$ is the Laplacian of the electron density, and $G\left(r_{\rm CP}\right)$ is the kinetic electron density, all at the critical point. Topological analyses of the

[1] Supporting information for this paper is available from the IUCr electronic archives (Reference: BI5017).

electron-density distributions were carried out using *AIM2000* (Biegler-König *et al.*, 2001). It should be stressed that a good agreement between the above expression and Hartree–Fock calculations of G is obtained only in the medium-range region, *i.e.* for distances in the range 0.5–2.1 Å from the atomic nuclei. Therefore, Espinosa *et al.* considered the above expression valuable for closed-shell interactions such as hydrogen bonds.

2.3.3. *PIXEL* calculations. The *CRYSTAL09* optimized structures were used to calculate the molecular electron density distribution by standard quantum-chemical methods using the *GAUSSIAN09* package at the MP2 (Møller & Plesset, 1934) /6-31G(d,p) level of theory. The electron density was then analysed using the *PIXEL* method (Gavezzotti, 2002, 2003*a*,*b*), which allows for the calculation of dimer ($E_{\rm D}^{\rm P}$) and lattice energies ($E_{\rm coh}^{\rm P}$). In the lattice-energy calculations, a cluster of molecules within a radius of 20 Å was used. The output yields the total lattice energy and its breakdown into electrostatic, polarization, dispersion and repulsion components.

2.4. TAAM refinement

The transferable aspherical atom model (TAAM) refinement method (Bąk *et al.*, 2009; Dittrich *et al.*, 2002, 2009; Jarzembska *et al.*, 2012; Jarzembska, Kamiński *et al.*, 2013; Volkov *et al.*, 2004, 2007) is based on aspherical atom charge density models kept in the Hansen–Coppens formalism (Hansen & Coppens, 1978). Such models imitate real atoms more reliably than the spherical approximation (IAM), and so may serve as more appropriate atomic scattering factors. The overall procedure consists of three main steps. Firstly, the IAM method is applied in the low-resolution experimental data refinement ($0.0 \leq \sin\theta/\lambda \leq 0.7$ Å^{-1}) to obtain initial molecular geometry and atomic displacement parameters for the purpose of the subsequent TAAM approach. In the IAM refinement the scale factor, atomic coordinates, anisotropic atomic displacement parameters of non-H atoms and isotropic atomic displacement parameters of H atoms, are refined. Then, with the obtained molecular geometry, adequate pseudoatom multipolar parameters can be either transferred from an independent source such as a database, or calculated theoretically. For this work, the University of Buffalo Pseudoatom Databank (UBDB) atom-type models were applied and the transfer of the pseudoatom parameters and the local coordinate system assignment were accomplished with the *LSDB* program (Jarzembska & Dominiak, 2011; Volkov *et al.*, 2004). To assure molecular electroneutrality (or, in general, to impose a given charge), the monopole populations of the pseudoatoms are scaled employing the Faerman & Price method (Faerman & Price, 1990). A structural refinement performed with these transferred aspherical atomic scattering factors constitutes the last step. During a standard

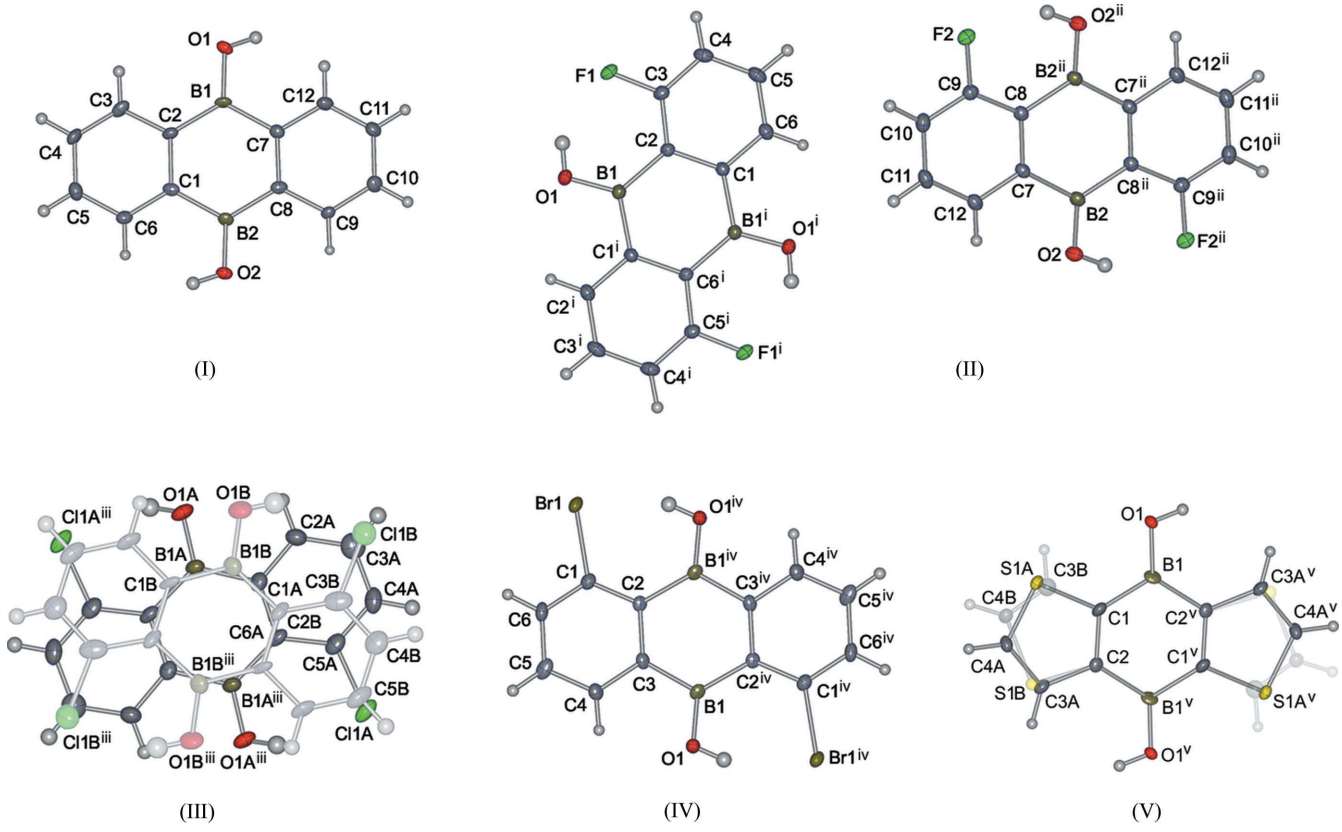

Figure 1
Atom-labelling scheme and atomic displacement parameters at 50% probability for non-H atoms. For (III) and (V), one of the disorder components is shown as semi-transparent. Symmetry codes: (i) $-x+1, -y+1, -z+1$; (ii) $-x, -y+2, -z+1$; (iii) $-x+2, -y+1, -z$; (iv) $-x+2, -y+1, -z+2$; (v) $-x+2, -y+1, -z+1$.

TAAM refinement procedure, an overall scale factor, atomic positions and ADPs are refined with reference to experimental data, while the multipolar populations and kappa values are fixed at databank values.

Since it was problematic to carry out TAAM refinements of equal quality for all structures (due to disorder or heavy atoms) we decided to apply this method solely to the structure of (II). Such a procedure allows for reconstruction of the electron density distribution in the structure, with our main interest being the deformation densities in the region of the F···F interactions. It is worth noting that in comparison with the IAM refinement, the residual electron density is significantly flattened after TAAM refinement (the minimum and maximum values of residual electron density being ± 0.14 e Å^{-3}).

3. Results and discussion

3.1. Molecular geometry

The crystal structures of (II), (III) and (IV) adopt the space group $P2_1/c$ [described in the $P2_1/n$ setting for (III) and (IV); Table 1], whereas (V) crystallizes in space group $R\bar{3}$. In (II) there are two crystallographically distinct molecules, each occupying on an inversion centre (Fig. 1). In (III), (IV) and (V) there is only one crystallographically distinct molecule occupying an inversion centre [disordered in the case of (III); Fig. 1]. Compound (I) appears as two polymorphic forms. The previously reported structure at 165 K (Januszewski *et al.*, 2011) is monoclinic with space group $P2_1/c$. Our structure, measured at 100 K, is characterized by non-centrosymmetric $P2_12_12_1$ space-group symmetry. All of the studied molecules are planar with the C—C bond lengths in the approximate range 1.37–1.42 Å, comparable to those of the anthracene (Ponomarev & Shilov, 1983) and anthraquinone (Fu & Brock, 1998). The B—C bond lengths (1.56–1.58 Å) are also comparable to those found in boronic and borinic acids (Hall, 2005). An important feature of (II), (III) and (IV) is the formation of an in-plane intramolecular O—H···*X* interaction.

3.2. Crystal structure of (I)

In the orthorhombic polymorph of (I), the O—H···O and C—H···O hydrogen-bond interactions [motif **H**: O1—H1···O2^{i} and C9^{i}—H9^{i}···O1; motif **H′**: O2—H2···O1^{ii} and C3^{ii}—H3^{ii}···O2, symmetry codes: (i) $-x, y-\frac{1}{2}, -z+\frac{1}{2}$; (ii) $-x+1, y+\frac{1}{2}, -z+\frac{1}{2}$; Fig. 2] link the molecules into chains which propagate along the [100] direction (Fig. 3). The geometrical and topological parameters of the most important interactions are summarized in Table 2. A rigid and planar framework of the boranthrene ring facilitates the formation of π-stacking between the B-containing and aromatic molecular fragments. Thus, in contrast to anthracene, where the supramolecular architecture is based on C—H···π contacts (Ponomarev & Shilov, 1983), the boranthrene molecules are

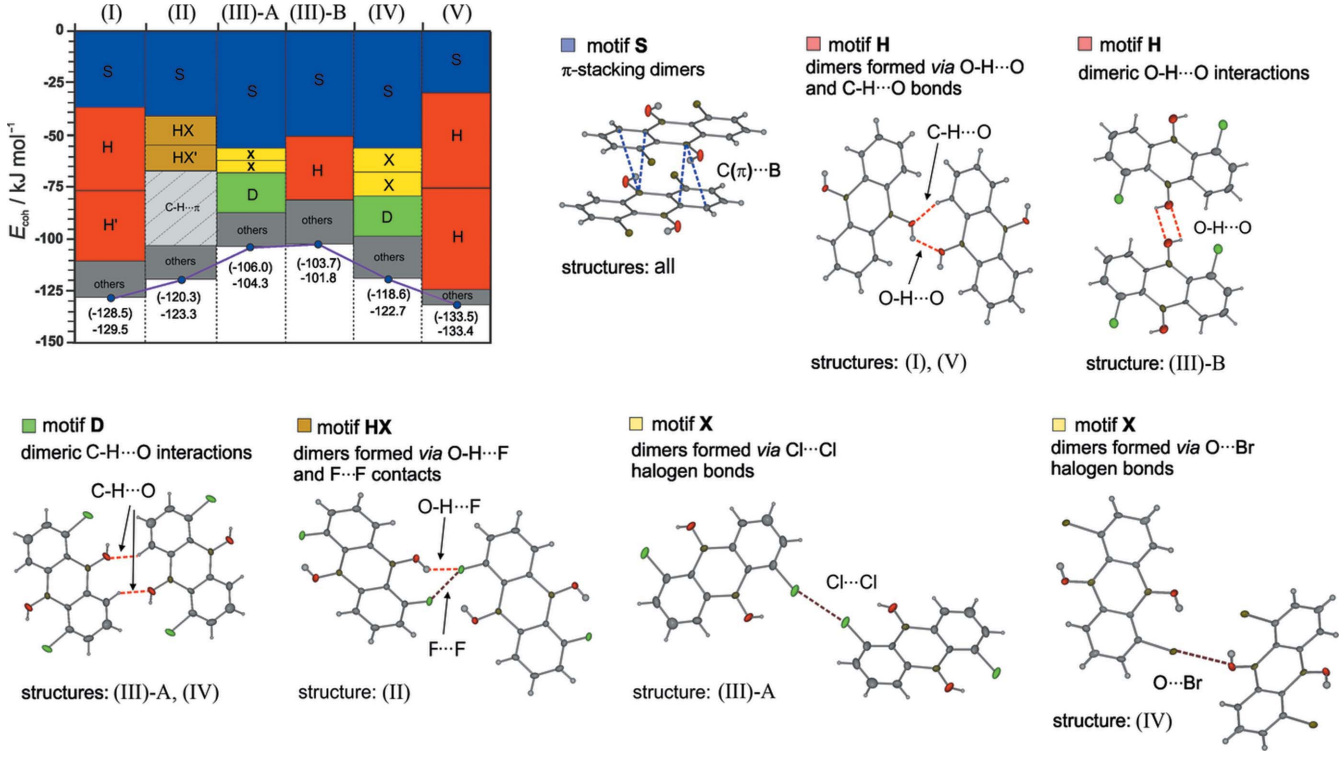

Figure 2
Comparison of cohesive (E^{P}_{coh}) and dimer (E^{P}_{D}) energy values calculated with *PIXEL* between the boranthrene molecules, together with schematic representatives of the corresponding dimers. The cohesive energy values obtained from *CRYSTAL09* (E^{C}_{coh}) are given in brackets. The motifs **H′** and **HX′** are similar to **H** and **HX**, and therefore they are not shown.

Table 2
Geometrical (Å,°) and topological parameters for dimers in the *CRYSTAL09* optimized crystal structure of (I)–(V).

ρ = electron density (e Å^{-3}), $\nabla^2\rho$ = Laplacian (e Å^{-5}), G = kinetic energy density (kJ mol^{-1} bohr^{-3}), V = potential energy density (kJ mol^{-1} bohr^{-3}), E_{top}^{G} = interaction energy derived from charge density topology (kJ mol^{-1}), E_D^G = dimer energy obtained using a supermolecular method implemented in *GAUSSIAN09* (B97D/aug-cc-pVTZ; kJ mol^{-1}), E_D^P = dimer energy derived from the *PIXEL* method (kJ mol^{-1}), **r**(BCP) denotes the position of the bond critical point.

	Motif	Interaction	$X\cdots A$	$D-X$	$D\cdots A$	$D-X\cdots A$	$\rho(\mathbf{r}_{BCP})$	$\nabla^2\rho\ (\mathbf{r}_{BCP})$	$G(\mathbf{r}_{BCP})$	$V(\mathbf{r}_{BCP})$	ΣE_{top}^{G}†	E_D^G	E_D^P
(I)	**H**	O1—H1···O2^{i}	2.08	0.97	2.895	145	0.122	1.73	40.9	−34.6	−29.1	−28.1	−32.2
		C9^{i}—H9^{i}···O1	2.25	1.08	3.281	159	0.097	1.20	28.2	−23.7			
	H′	O2—H2···O1^{ii}	2.01	0.97	2.861	145	0.139	2.00	48.0	−41.4	−33.7	−29.0	−33.5
		C3^{ii}—H3^{ii}···O2	2.28	1.08	3.254	160	0.103	1.31	30.9	−26.2			
(II)	**HX**	O1—H1···F1^{ii}	2.29	0.97	3.092	140	0.060	0.93	19.7	−14.2	−7.1	−10.0	−12.1
		F1···F1^{ii}	–	–	2.947	–	0.039	0.70	14.2	−9.1	–		
	HX′	O2—H2···F2^{iii}	2.05	0.97	2.848	139	0.106	1.67	37.8	−30.0	−15.0	−13.0	−14.9
		F2···F2^{iii}	–	–	2.825	–	0.054	0.91	18.9	−13.1	–		
(III)-*A*	**D**	C6—H6···O1^{iv}	2.58	1.08	3.337	127	0.046	0.59	12.5	−9.0	−9.0‡	−15.2	−18.9
	X	Cl···Cl^{v}	–	–	3.486	–	0.043	0.61	12.7	−8.9	–	−3.2	−4.4
(III)-*B*	**H**	O1—H1···O1^{iv}	2.28	0.97	2.717	106	0.094	1.70	37.0	−27.6	−27.6‡	−25.3	−27.9
(IV)	**D**	C5—H5···O1^{vi}	2.72	1.09	3.728	154	0.036	0.43	9.0	−6.4	−6.4‡	−17.4	−21.5
	X	O1···Br1^{vii}	–	–	3.266	–	0.047	0.64	13.6	−9.7	–	−9.9	−9.8
(V)	**H**	O1—H1···O1^{viii}	1.71	0.99	2.674	164	0.267	3.68	101.5	−102.5	−57.9	−41.9	−42.3
		C3*A*—H3*A*···O1^{viii}	2.49	1.08	3.425	144	0.065	0.73	17.3	−13.8			

Symmetry codes: (i) $-x, y-\frac{1}{2}, -z+\frac{1}{2}$; (ii) $-x+1, y+\frac{1}{2}, -z+\frac{1}{2}$; (iii) $x, -y+\frac{3}{2}, z+\frac{1}{2}$; (iv) $x-1, y-1, z$; (v) $-x-\frac{1}{2}, y-\frac{1}{2}, -z+\frac{1}{2}$; (vi) $-x+1, -y+1, -z+1$; (vii) $x+\frac{1}{2}, -y+\frac{1}{2}, z+\frac{1}{2}$; (viii) $-y+\frac{1}{3}, x-y-\frac{1}{3}, z-\frac{1}{3}$. † E_{top}^{G} values are estimated only in the case of hydrogen bonds (O—H···O, C—H···O, O—H···F). ‡ Contribution from two interactions are taken into account.

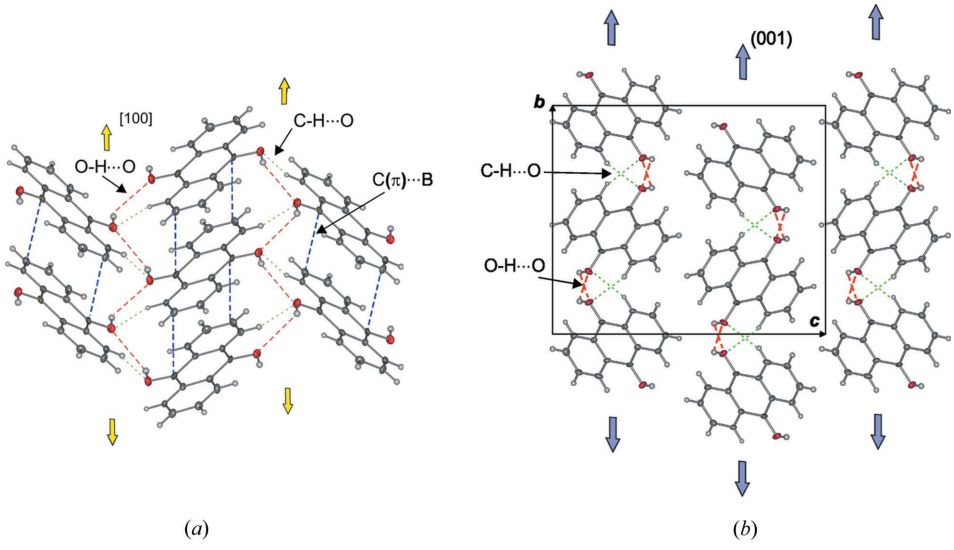

Figure 3
(*a*) The [100] hydrogen-bonded chains in the structure of (I) (orthorhombic polymorph) and (*b*) their further aggregation into layers parallel to (001). O—H···O contacts are shown as red dashed lines, C—H···O as green dotted lines, and π-stacking contacts as blue dashed lines.

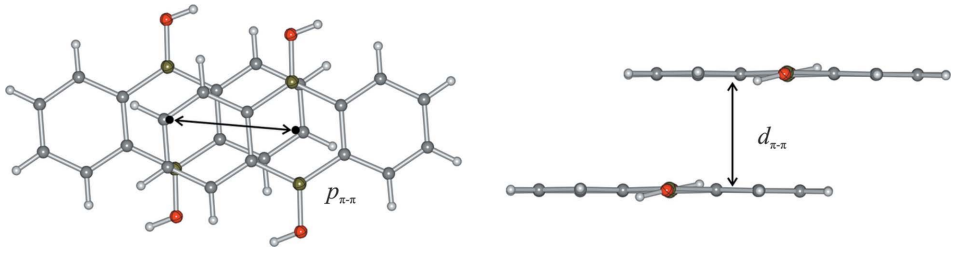

Figure 4
Example of a π-stacked dimer (denoted motif **S**), with the definition of $p_{\pi-\pi}$ and $d_{\pi-\pi}$.

parallel, providing efficient contacts between the B and aromatic C atoms. In (I) the interplanar distance ($d_{\pi-\pi}$) between the stacked dimers is 3.31 Å. The C(π)···B contacts are formed with the γ-C atoms, which leads to a significant horizontal displacement of parallel-oriented molecules ($p_{\pi-\pi}$ = 3.67 Å). The geometries of the π-stacking interactions and energies of the interacting dimers are listed in Table 2, while the π-stacking molecules and definitions of $p_{\pi-\pi}$ and $d_{\pi-\pi}$ are shown in Fig. 4.

The structure of the previously published monoclinic polymorph of (I) (Januszewski *et al.*, 2011) is characterized by a very similar crystal network, with a layered architecture. In the orthorhombic structure, all molecules are equivalent by symmetry (Z' = 1), while the monoclinic polymorph contains two independent molecules in the asymmetric unit, each occupying a crystallographic inversion centre ($Z' = \frac{1}{2} + \frac{1}{2}$). The two polymorphs contain identical layers (corresponding to the two chains of molecules shown within the unit cell in Fig. 3*b*), but they differ in the orientation of molecules between the layers (see the figure in the supporting information).

Concerning geometrical parameters, the O—H···O hydrogen-bond interactions in both polymorphs seem to be relatively weak: (I) (orthorhombic, 100 K): O1···O2 = 2.861 Å, O1—H1···O2 = 144.5°; O2···O1 = 2.895 Å, O2—H2···O1 = 144.7°; (I) (monoclinic, 165 K): O1···O2 = 3.024 Å, O1—H1···O2 = 158.6°, O2···O1 = 3.044 Å, O2—H2···O1 = 151.9° (geometries refer to the *CRYSTAL09* optimized structures). This is also clearly visible on the corresponding Hirshfeld surface generated for the orthorhombic polymorph (Spackman & Byrom, 1997; McKinnon *et al.*, 1998) (Fig. 5). The fingerprint plot shows that the symmetric O—H···O spikes, commonly observed in other structures (McKinnon *et al.*, 2004), are quite short and hardly distinguished. On the other hand, the theoretical calculations show that the hydrogen bonds are of moderate strength. On the basis of the electron-density distribution calculated for the **H** and **H′** motifs (Table 2), the bond critical point densities, $\rho(\boldsymbol{r}_{\rm BCP})$, for the O—H···O bonds are equal to 0.122 and 0.139 e Å^{-3}, and the Laplacian, $\nabla^2\rho$ ($\boldsymbol{r}_{\rm BCP}$), equal to 1.73 and 2.00 e Å^{-5}, respectively. According to the Espinosa–Lecomte estimation, the corresponding interaction energies ($E^{\rm G}_{\rm top}$) are −17.3 and −20.7 kJ mol^{-1}, which is comparable to the strength of the hydrogen bonds in water (−20 kJ mol^{-1}; Durka *et al.*, 2012; Feyereisen *et al.*, 1996; Gu *et al.*, 1999). It should be noted that these values are also similar to the binding energies of single hydrogen-bonded dimers of 2,3-difluorophenylene-1,4-diboronic acid (−23.4 kJ mol^{-1}; Durka *et al.*, 2012). However, as will be discussed in detail (§§3.6 and 3.7), the hydrogen interactions in (I) are weaker compared with the thiophene analogue (V). The weakening of the O—H···O hydrogen bond in (I) can be simply understood taking into account that the OH groups are sterically hindered by the β-H atoms, which prevent molecules from approaching each other at the distance to allow for stronger hydrogen bonding. For (II)–(IV) the halogen substitution at the C1 and C6 positions will amplify this effect.

A higher structural diversity resulting from the flexibility of the O—H···O bonds facilitates the occurrence of other competitive interactions. For instance, in (I) the O—H···O hydrogen-bond interactions compete with C—H···O (their estimated interaction energies amount to −11.8 and −13.1 kJ mol^{-1} for motifs **H** and **H′**, respectively). The sum of the O—H···O and C—H···O energy values is quite well reproduced by the dimer energy obtained from the *GAUSSIAN09* and *PIXEL* calculations ($E^{\rm G}_{\rm D}$ and $E^{\rm P}_{\rm D}$ values in Table 2).

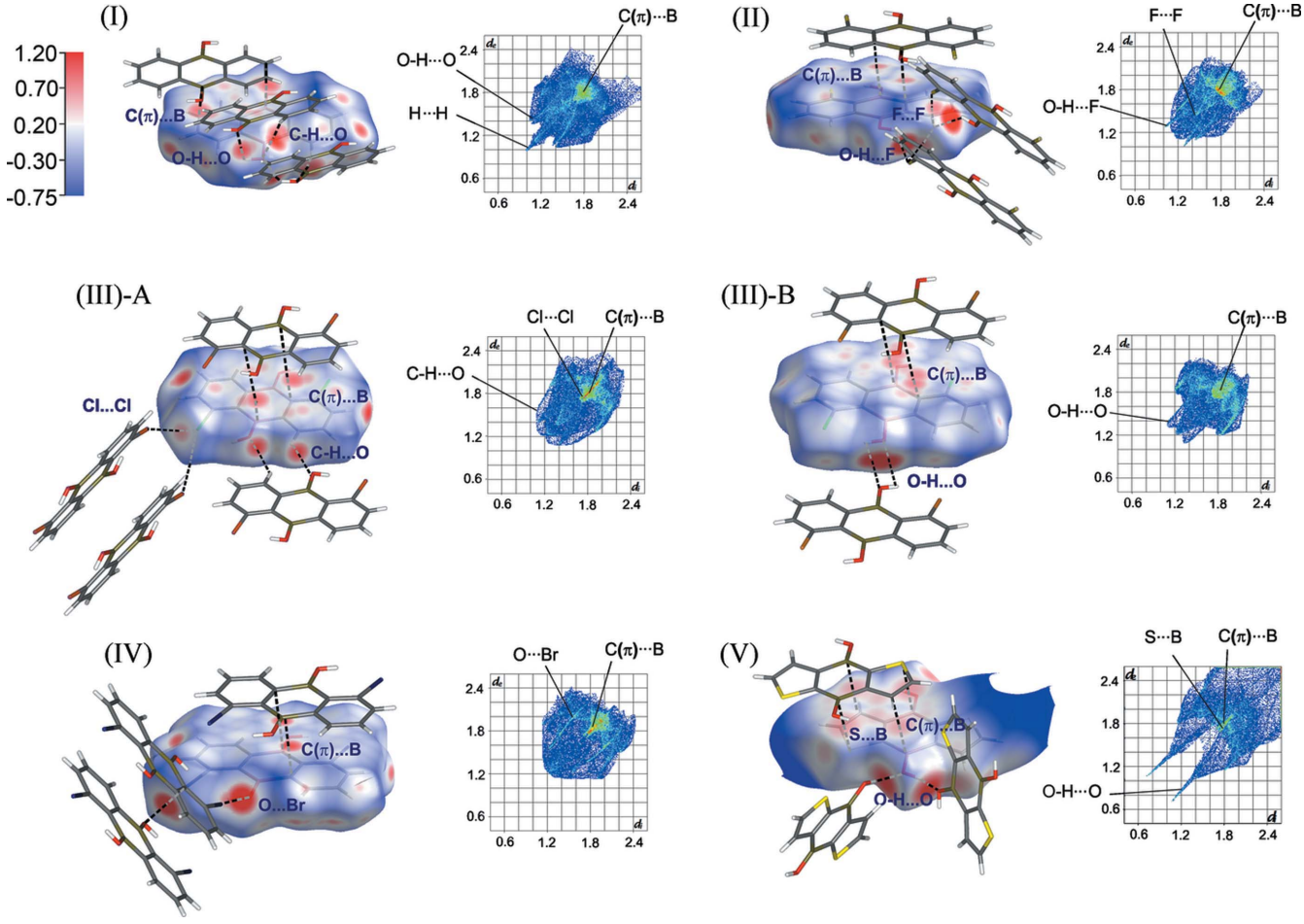

Figure 5
Hirshfeld surfaces together with the corresponding fingerprint plots generated for (I)–(V), with the $d_{\rm norm}$ property mapped in the range from −0.75 to 1.20. Selected neighbouring molecules and weak interactions are additionally shown. Generated using *CrystalExplorer* (Turner *et al.*, 2011).

Table 3
Geometrical parameters (Å, °) and energy values of π-stacked dimers (motif **S**) in the *CRYSTAL09* optimized structures of (I)–(V).

E_D^G = dimer energy obtained using a supermolecular method with *GAUSSIAN09* (B97D/aug-cc-pVTZ) (kJ mol^{-1}), E_D^P = dimer energy derived from the *PIXEL* method (kJ mol^{-1}).

	Motif	Interaction	C(π)···B	$d_{\pi-\pi}$	$p_{\pi-\pi}$	E_D^G	E_D^P
(I)	**S**	C4···B2^{i}	3.575	3.312	3.671	−38.1	−37.6
		C5···B2^{i}	3.329				
		C6···B2^{i}	3.519				
		C10^{ii}···B1	3.628				
		C11^{ii}···B1	3.359				
		C12^{ii}···B1	3.520				
(II)	**S**	C1···B1^{iii}	3.539	3.401	1.647	−46.6	−41.1
		C2···B1^{iii}	3.526				
	S′	C7···B2^{iv}	3.385	3.354	1.741	−46.6	−42.2
		C8···B2^{iv}	3.507				
(III)-*A*	**S**	C2···B1^{iv}	3.364	3.369	1.904	−60.7	−55.4
		C3···B1^{iv}	3.445				
(III)-*B*	**S**	C1···B1^{iv}	3.444	3.419	1.813	−52.2	−49.4
		C2···B1^{iv}	3.502				
(IV)	**S**	C2···B1^{iv}	3.544	3.389	1.940	−60.3	−55.3
		C3···B1^{iv}	3.358				
		C4···B1^{iv}	3.600				
(V)	**S**	C3*A*···B1^{iii}	3.349	3.388	3.211	−30.0	−27.5
		S1*A*···B1^{v}	3.421				

Symmetry codes: (i) $x+1, y, z$; (ii) $-y+\frac{1}{3}, x-y-\frac{1}{3}, z-\frac{1}{3}$; (iii) $-x+1, -y+1, -z+1$; (iv) $x, y-1, z$; (v) $-x+\frac{2}{3}, -y+\frac{1}{3}, -z+\frac{1}{3}$.

3.3. Crystal structure of (II)

The two independent molecules in the asymmetric unit of (II) are denoted (II)-*A* and (II)-*B*. The crystal packing of this compound, illustrated in Fig. 6, is based on O—H···F and F···F contacts connecting molecules into chains along [010]: motif **HX**: O1—H1···F1^{ii} and F1···F1^{ii}; motif **HX′**: O2—H2···F2^{iii} and F2···F2^{iii} [symmetry codes: (ii) $-x+1, y+\frac{1}{2}, -z+\frac{1}{2}$; (iii) $x, -y+\frac{3}{2}, z+\frac{1}{2}$]. The inter-F distance within the (II)-*A*/(II)-*A* dimer (motif **HX**) is 2.947 Å, and 2.825 Å within the (II)-*B*/(II)-*B* dimer (motif **HX′**), whereas O···F = 3.092 (motif **HX**) and 2.848 Å (motif **HX′**) (geometries refer to the *CRYSTAL09* optimized structures).

The O—H···F and F···F contacts are also well visible on the Hirshfeld surfaces (Fig. 5): two primary bright red spots (*i.e.* short contacts) located near to the F atoms correspond to the O—H···F interactions, while two weaker spots found nearby correspond to the F···F contacts. The topological analysis shows that the most important contribution to the **HX** dimer energies comes from the O—H···F hydrogen bond. The estimated E_{top}^G values for these contacts are −7.1 and −15.0 kJ mol^{-1} for **HX** and **HX′**, respectively. The reason for the absence of O—H···O hydrogen-bond interactions in this structure is not clear. It should be noted that in the crystal structure of the related system 8-fluoro-4-methyl-1-naphthol, featuring the OH and F groups at the C1 and C8 positions of the naphthalene ring, both O—H···O and O—H···F hydrogen bonds are formed (Takemura *et al.*, 2009).

In contrast to structure (I), the C(π)···B interactions in (II) are formed with the α-C atom, which provides a very efficient stacking (Table 3). A similar pattern of π-stacking contacts occurs in the structure of anthraquinone (Fu & Brock, 1998) and the closer analogue 5,10-dibromo-5,10-dihydroboranthrene (Januszewski *et al.*, 2011).

The F···F contacts are shorter than 2.95 Å (twice the van der Waals radius for F) and can formally be considered as halogen-bond interactions. The role of F interactions in crystal engineering and the ability of so-called 'organic F atoms' to participate in intermolecular interactions have been a matter of recent discussions (Berger *et al.*, 2011; Chopra, 2012; Chopra *et al.*, 2005; Collas *et al.*, 2010; Feyereisen *et al.*, 1996; Hathwar, Gonnade *et al.*, 2011; Hathwar & Row, 2011, Mariaca *et al.*, 2006; Metrangolo *et al.*, 2011; Murray *et al.*, 2009; Politzer *et al.*, 2008; Reichenbächer *et al.*, 2004; Schwarzer *et al.*, 2004; Schwarzer & Weber, 2008; Stammler *et al.*, 2013). The F atom has a relatively small size, high electronegativity and very low polarizability, and hence does not exhibit a strong tendency to form halogen-bond interactions. Despite numerous reports showing the importance of various contacts with F atoms (O—H···F, N—H···F, C—H···F, F···F or F···π), their nature remains controversial. Taking into account geometrical parameters, the C—*X*···*X*—C (*X* = F, Cl, Br, I) halogen-bond interactions have been classified into two subgroups: type I when both C—*X*···*X* angles are equal, and type II when one C—*X*···*X* angle is close to 180° and the other to 90° (Pedireddi *et al.*, 1994; see the scheme in the supporting information). It has been concluded that F atoms prefer type I contacts. In the structure of (II) the C—F···F angles are close to 115 and 150°, and therefore cannot be categorized into any of the above-mentioned groups. However, according to the Politzer results (Murray *et al.*, 2009; Politzer *et al.*, 2008), the geometrical arrangement

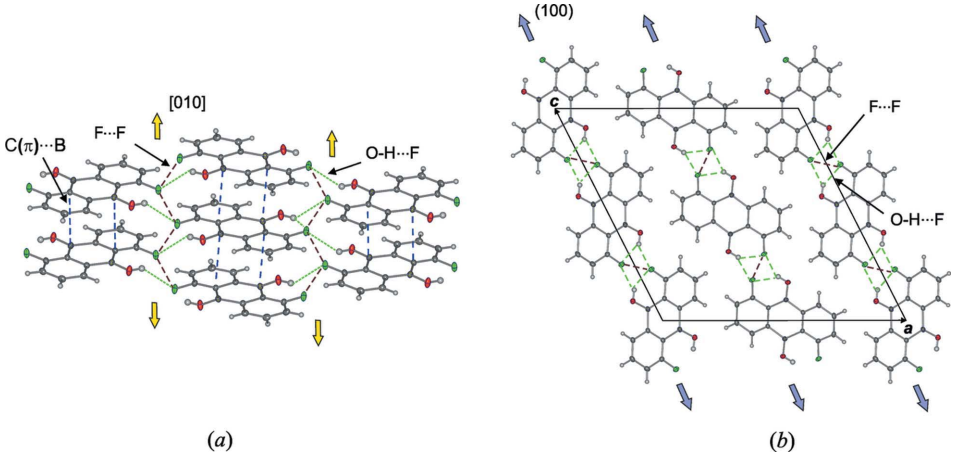

Figure 6
(*a*) Molecular layers and (*b*) their further aggregation in (II). Intermolecular O—H···F and F···F interactions are marked as green and brown lines, respectively, and π-stacking contacts as blue dashed lines. The yellow and blue arrows show the direction of (*a*) chains and (*b*) layers.

of the groups involved in halogen-bonding interactions seems to result from the electrostatic potential properties. Therefore, the distributions of geometrical parameters are likely to be scattered between the two idealized cases. This seems to be confirmed by the results of a Cambridge Structural Database (CSD; Allen, 2002) search (see the supporting information).

To gain a deeper insight into the nature of the F···F interaction, we have used the TAAM refinement procedure (details are described in §2). It allows for reconstruction of the electron density distribution in the structure of (II). Recent studies have shown that such a method provides a good estimation of experimental charge density (Bąk *et al.*, 2009; Jarzembska, Goral *et al.*, 2013; Jarzembska, Kamiński *et al.*, 2013). The deformation density map of (II) shows the anisotropic distribution of electron density around the F atoms (Fig. 7). The topological analysis of the electron density within motifs **HX** and **HX′** indicates that there is a bond critical point (BCP) between the F atoms. The $\rho(\mathbf{r}_{BCP})$ values (0.039 and 0.054 e Å^{-3} for the F1···F1 and F2···F2 contacts, respectively) are very small, $\nabla^2\rho(\mathbf{r}_{BCP})$ are positive (0.70 and 0.91 e Å^{-5} for F1···F1 and F2···F2, respectively) and the $|V(\mathbf{r}_{BCP})|/G(\mathbf{r}_{BCP})$ values are less than 1, which represents closed-shell interactions. These values are similar to those found in other structures featuring close F···F contacts (Bach *et al.*, 2001; Hathwar, Gonnade *et al.*, 2011; Hathwar & Row, 2011). However, the exact nature of the F···F contact still is not clear. The anisotropic distribution of electron density around the F atom may reduce repulsions between the valence electron densities, allowing two F atoms to come closer than the sum of their van der Waals radii. Therefore, the bond path and BCP along the F···F contact may result from local stabilization, and it may be regarded as a repulsive non-bonding interaction.

3.4. Crystal structure of (III)

In the chloro-substituted derivative (III), the residual electron density map reveals molecular disorder (see the figure in the supporting information). The refinement shows that there are two different orientations of the molecule, denoted (III)-*A* and (III)-*B*, with site occupancy factors *ca* 0.6:0.4 (at 100 K). Both molecular components are located in the same plane, and occupy a crystallographic inversion centre. The two components are related by a local twofold rotation axis within the molecular plane, passing through the inversion centre, and bisecting the positions of atoms B1*A* and B1*B* (vertical in Fig. 1).

The observed static disorder may originate from a variety of different supramolecular assemblies which may appear in the crystal structure. The crystal may exhibit a domain structure composed of fragments built exclusively by molecules (III)-*A* (domain *A*) or (III)-*B* (domain *B*), or it may contain a random distribution of both sites in various stoichiometric proportions (as in a solid solution). When the two domains are considered independently, molecules in domain *A* form halogen-bond interactions with a Cl···Cl distance equal to 3.486 Å (motif **X**). This leads to the formation of (101) layers as shown in Fig. 8(*a*) (yellow arrows). The O atoms are involved in dimeric C—H···O interactions (motif **D**), which leads to the formation of [001] chains (Fig. 8*a*, red arrows). A completely different supramolecular assembly is found in domain *B*. The hydroxyl groups are mutually arranged to form symmetric O—H···O hydrogen bonds (see motif **H**), with O···O = 2.717 Å. This leads to the formation of the [100] molecular chains (Fig. 8*b*, blue arrows).

The molecular Hirshfeld surfaces generated for molecules (III)-*A* and (III)-*B* in their own environments have quite similar shapes, but differently localized hotspots, reflecting different intermolecular arrangements. The surface of (III)-*A* shows four primary spots, two of them corresponding to the dimeric C—H···O contacts, one to the Cl···Cl interaction, and one to a relatively short C—H···H—C contact. In turn, the molecular Hirshfeld surface of (III)-*B* shows only one, but quite intense, spot corresponding to the O—H···O hydrogen bond. The molecules at the (III)-*A* and (III)-*B* sites are additionally held together by stacking C(π)···B contacts, as observed in the other structures. In both cases, the shortest π-stacking contacts are formed between the B atom and the α-C atom of the neighbouring molecule.

Topological analysis of the electron density distribution reveals that the BCP between the Cl atoms is characterized by a small value of $\rho(\mathbf{r}_{BCP})$ (0.043 e Å^{-3}) and a positive value of $\nabla^2\rho(\mathbf{r}_{BCP})$ (0.61 e Å^{-5}). The interaction energy for this dimer is also quite small and amounts to approximately −4 kJ mol^{-1}. A more significant contribution to the total cohesive energy comes from the **D** motif formed by the two dimeric C—H···O contacts (E_D^G = −15.2; E_D^P = −18.9 kJ mol^{-1}). In the case of the **H** dimers, there are two close BCPs between the OH groups. The **H** motif energy values obtained from the *GAUSSIAN09* and

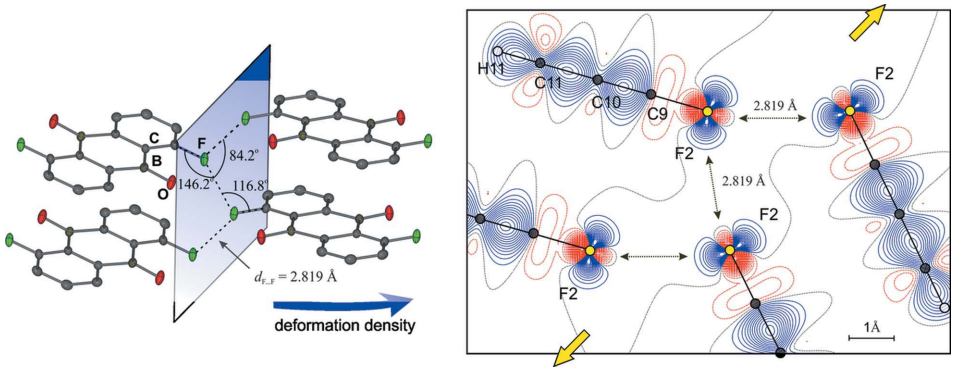

Figure 7
The geometry of F···F interactions and the static deformation density map derived from the TAAM refinement (0.05 e Å^{-3} contours, blue solid lines: positive, red dashed lines: negative, grey dashed lines: zero). Deformation density maps were produced with *MOPRO* (Jelsch *et al.*, 2005).

PIXEL calculations (E_D^G = −25.3; E_D^P = −27.9 kJ mol^{-1}) are well reproduced by the sum of the Espinosa–Lecomte estimated value (E_{top}^G = −27.6 kJ mol^{-1}).

The computational results show that the (III)-*A* and (III)-*B* molecules are equally well stabilized in the environments of their counterparts (see the figure in the supporting information). The roughly estimated overall interaction energy of these molecules with their closest surrounding neighbours leads to a minor difference of 2 kJ mol^{-1} between the two complementary situations [*i.e.* −170.3 kJ mol^{-1} in the case of (III)-*A* in the surroundings of the (III)-*B* molecules, and −172.2 kJ mol^{-1} for the opposite arrangement]. Thus, any mixed arrangements can be formed. For instance, an alternating arrangement of molecules (III)-*A* and (III)-*B* leads to the formation of O—H···O and C—H···O hydrogen-bonded chains (Figs. 8*c* and *d*). It is noticeable that a similar pattern of hydrogen-bond interactions is observed in (I).

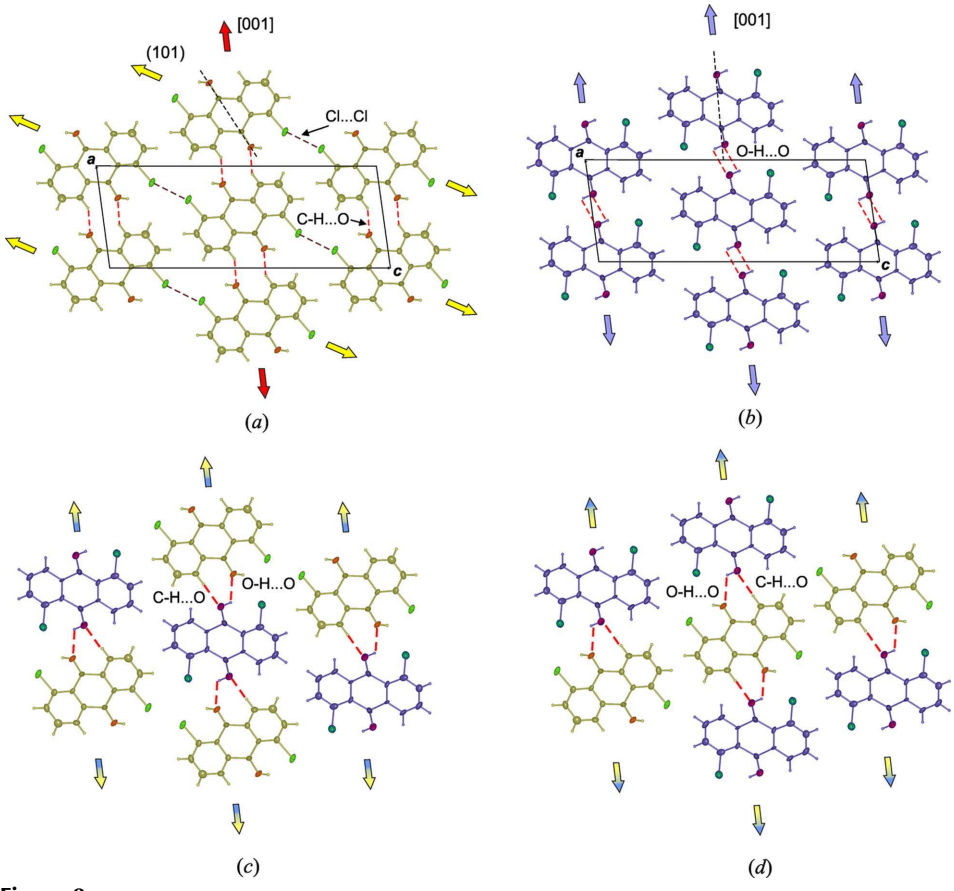

Figure 8
Packing diagrams of (III) showing the supramolecular architecture within the domains: (*a*) *A* and (*b*) *B*, formed exclusively by molecules in site (III)-*A* and (III)-*B*, respectively. (*c*), (*d*) The mixed arrangements are dominated by O—H···O and C—H···O chains.

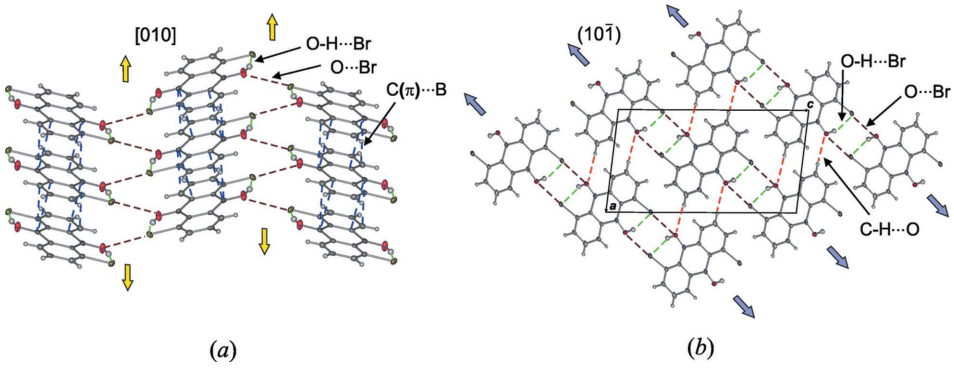

Figure 9
(*a*) Molecular layers and (*b*) their further aggregation in (IV). The Br···O interactions are marked as brown, and C(π)···B interactions as blue dashed lines.

3.5. Crystal structure of (IV)

The structure of (IV) is dominated by Br···O halogen-bonding interactions (motif **X**), which link molecules into [010] chains (Fig. 9). The Br···O distance is 3.226 Å, which is shorter than the sum of the Br and O van der Waals radii (3.35 Å). The pattern of the π-stacking contacts is similar to that in the structure of (III). The $\rho(\boldsymbol{r}_{BCP})$ and $\nabla^2\rho(\boldsymbol{r}_{BCP})$ values at the BCP of the O···Br interaction are 0.047 e Å^{-3} and 0.64 e Å^{-5}, respectively, and the dimer energy is equal to about −10 kJ mol^{-1}. Additionally, the network is linked by C—H···O interactions within the dimeric **D** motifs.

3.6. Crystal structure of (V)

The structure of (V) is based mainly on O—H···O interactions (**H** motif). Each OH group acts as a donor and acceptor of a hydrogen-bond interaction, forming an α-helix consisting of repeated triplets of molecules (Fig. 10*a*). In such triplets, the dihedral angle between the mean planes of two neighbouring molecules is 72.2°. The parallel molecules from adjacent triplets participate in π-stacking interactions formed between the B-containing molecular fragment and the more electronegative S and C atoms. The distance between the stacked planes is equal to 3.39 Å, which is the shortest within the structures of (I)–(V). The hydrogen-bond interaction (O···O = 1.714 Å, O—H···O = 163.8°) is much stronger and more directional than that observed in the structures of (I) and (III)-*B*. This is also reflected in the topological

parameters at the BCP of O—H···O: $\rho(\boldsymbol{r}_{BCP})$ = 0.267 e Å^{-3}; $\nabla^2\rho(\boldsymbol{r}_{BCP})$ = 3.86 e Å^{-5}. It should be noted that the energy of this interaction derived from topological parameters may be overestimated (E^{G}_{top} = −57.9 kJ mol^{-1}) as it is significantly higher than the dimer interaction energies derived from *PIXEL* and *GAUSSIAN09* calculations (E^{G}_{D} = −41.9; E^{P}_{D} = −42.3 kJ mol^{-1}). Nevertheless, the significant amplification of the hydrogen-bond interaction in (V) is due to the fact that the molecules are smaller and significantly twisted relative to their neighbours, and therefore more compact hydrogen-bonded chains are formed. Moreover, in the five-membered thiophene ring, the OH groups are not shielded by the H or halogen atom at the β-position, as in (I)–(IV), allowing neighbouring molecules to come closer and form stronger hydrogen-bond interactions.

The antiparallel chains in (V) form a special three-dimensional network that contains opened channels (Fig. 10*b*). The accessible diameter of the hexagonal channels defined by the van der Waals radii of the framework atoms (Bondi, 1964) is approximately 5.38 Å. Calculations performed with *PLATON* (Spek, 2009) show that the channel volume is equal to 446.1 Å^3 (per unit cell), which constitutes 18.1% of the total unit-cell volume. Visualization of the crystal voids is presented in the supporting information. Some residual electron density was found within the channels (handled by the *SQUEEZE* procedure during refinement), and the ^{1}H NMR spectrum of (V) also provides evidence for the presence of a small amount of included solvent molecules. Despite the presence of open channels, (V) does not exhibit any significant adsorption of gases (*ca* 0.04 wt% of H_2 and 0.3 wt% of N_2 at 77 K).

3.7. Comparison of the structures

The computations of cohesive energies performed in *PIXEL* and *CRYSTAL09* show that the structures of the non-halogen substituted molecules (I) and (V) are energetically most favoured among the series [E^{C}_{coh} = −128.5 and −133.5 kJ mol^{-1} for (I) and (V), respectively]. The halogen-containing structures (II) and (IV) are characterized by similar cohesive energy values (*ca* −120 kJ mol^{-1}). The comparable cohesive energy values of structures derived from the (III)-*A* and (III)-*B* domains (*ca* −100 kJ mol^{-1}) explain their simultaneous occurrence in one crystal lattice. A slightly more stabilizing energy value for the domain derived from (III)-*A* is in good agreement with the experimentally obtained higher occupancy ratio. The cohesive and dimer energies are summarized in Fig. 2.

The π–π stacking, hydrogen bonds (O—H···O, O—H···F and C—H···O) and halogen interactions (Cl···Cl, Br···O) play a dominant role in the crystal packing. The π–π dimer interaction energy depends on the distances between the mean planes of the stacking molecules ($d_{\pi-\pi}$) and also their mutual displacement ($p_{\pi-\pi}$). For instance, in the case of (III)-*A*, (III)-*B* and (IV), where C(π)···B contacts are formed between the B and α-C atoms ($p_{\pi-\pi}$ = 1.6–2.0 Å), the dimer interaction energies (both E^{G}_{D} and E^{P}_{D} values, Table 3) are the most stabilizing and correlate well with the interplanar distances $d_{\pi-\pi}$. In the case of (II) the π-stacking contacts are less efficient, which results in a decrease of the interaction energies. Finally, the dimer interaction energy is least stabilizing for (I) and (IV), where the displacement parameter $p_{\pi-\pi}$ is largest.

The crystal motifs and fingerprint plots illustrated in Fig. 5 allow division of the structures of (I)–(V) into two subgroups. In the first group, comprising (I), (III)-*B* and (V), the molecules form O—H···O hydrogen bonds within the **H** motifs. The second group, comprising (II), (III)-*A* and (IV), arises from motifs **X** and **HX**, dominated by interactions involving the halogen atom [O—H···F in (II), Cl···Cl in (III)-*A*, and O···Br in (IV)]. These are additionally supported by dimeric C—H···O [(III)-*A*, (IV)] hydrogen-bond interactions (motif **D**). In the first group, a significant contribution to the total cohesive energy comes from the O—H···O bonded dimers. This is reflected in the greater contribution of the electrostatic and polarization component to the total crystal lattice stabilization energy. What is noticeable on the Hirshfeld fingerprint plots is that the characteristic symmetric spikes derived from the O—H···O interactions are only found for (V), whereas for (I) and (III)-*B*, they are quite short and hardly distinguishable. This is accompanied by an elongation of the intermolecular O···O distances, reflecting a reduction of the degree of directionality and strength of the hydrogen bonds (Table 2). The weakening of the O—H···O bonds is caused by shielding of the OH groups by the

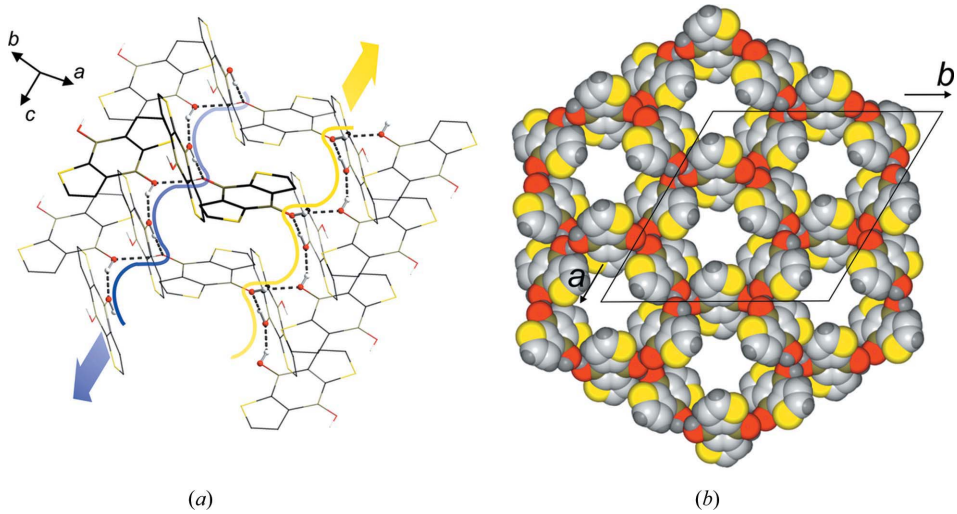

(*a*) (*b*)

Figure 10
(*a*) A network constructed from (V), showing the α-helical hydrogen-bond arrangement. The two adjacent helices are parallel, but oriented in opposite directions. (*b*) Hexagonal channels viewed along the *c* axis.

H atoms or more bulky halogen atoms in the β-position. In the five-membered thiophene ring of (V), the H atoms are further from the OH groups, and their impact on the O—H···O interactions is less relevant. It is noticeable that the high flexibility of the O—H···O hydrogen bond is also reflected in the strength of the competing C—H···O interactions. In (I), the energy of those bonds is about -12 kJ mol^{-1}, whereas in (V) it is -7 kJ mol^{-1}.

In the case of the second group, (II), (III)-*A* and (IV), the polarization energy component is the most significant contribution to the lattice energy. This is rationalized by the dominance of π–π stacking and halogen-type contacts. The Br atom, being the most polarizable, is expected to create the most advantageous halogen interaction. Indeed, the Br atom interacts with the more electronegative O atom and forms short Br···O contacts. The energy of such a dimer is equal to about -10 kJ mol^{-1}. The relevant contribution to the lattice energy of (IV) comes from the C—H···O bonded dimers (motif **D**), the energy of which is about -20 kJ mol^{-1}. Switching to a less polarizable Cl atom, the situation becomes more complex as there are two competitive structural motifs with comparable interaction energies. In the case of the domain (III)-*A*, the structure is based on a quite strong C—H···O interactions, which is reflected in the high stabilizing interaction energy value of $E_D^G = -15.2$ kJ mol^{-1} ($E_D^P = -18.9$ kJ mol^{-1}), and two Cl···Cl bonded dimers (motif **X**), which contribute about -4 kJ mol^{-1} to the total lattice energy. In turn, in the case of the domain built exclusively by the (III)-*B* molecules, all of those contacts are equivalent to the O—H···O interacting dimers ($E_D^G = -25.7$; $E_D^P = -27.9$ kJ mol^{-1}). The most unexpected motifs are observed for the structure of (II). Instead of the O—H···O hydrogen-bond interactions, the structure is based on synthons formed *via* O—H···F interactions. Moreover, in this case numerous weak C—H···π and other van der Waals contacts are observed which constitute a significant contribution to the total lattice energy.

4. Conclusions

Determination of the crystal and molecular structures of a series of boranthrenes shows the role and competitive/cooperative effects of halogen and hydrogen-bond interactions. The substitution of the halogen atom at the β-C atom leads to a significant change in the nature of crystal packing. As observed in the structure of the unsubstituted derivative (I), the O—H···O interactions are weakened due to the shielding of the OH groups by the β-H atoms, which further rationalizes the dominating role of halogen contacts in the remaining structures. Lack of such steric hindrance in (V) leads to the formation of a porous hydrogen-bonded organic framework. It is noticeable that the structures of the related 2-halophenols do not resemble this tendency (Kirsop *et al.*, 2004; Oswald, Allan, Motherwell & Parsons, 2005; Oswald, Allan, Day *et al.*, 2005). In all of those structures, the packing is based on hydrogen-bond interactions, and contacts with halogen atoms are rare.

The most energetically favoured dimers are formed by the π-stacking (for all structures) and O—H···O interactions [(I), (III)-*B*, (V)]. In the structures of (III)-*A* and (I), the O—H···O hydrogen bonds are substituted by halogen contacts supported by the C—H···O interactions. In the structure of the bromo-substituted derivative, the Br···O short contacts link molecules into chains. Also, a less polarizable Cl atom is involved in halogen-bonded aggregates in (III)-*A*. However, in this case the interaction energy of the Cl···Cl bonded dimer together with the energy of the auxiliary C—H···O bonded dimers is comparable to the energy values of the O—H···O bonded dimers in (III)-*B*. This leads to the formation of two different structural assemblies. Furthermore, our theoretical calculations show that molecules (III)-*A* and (III)-*B* are equally well stabilized in their counterpart's environments. The structures built by equimolar amounts of (III)-*A* and (III)-*B* in an alternating arrangement are stabilized by O—H···O and C—H···O interactions similar to those found in the structure of (I). This indicates that (III) can possess either a domain architecture composed of (III)-*A* and (III)-*B* domains, or a mixed arrangement with random or short-range ordered molecular orientations. It is, however, still unclear how the crystallization process affects the formation of particular crystal entities. Further crystallization experiments, carried out under the same conditions as the initial one, resulted in random (III)-*A* to (III)-*B* ratios (for instance, we observed 9:1), and we are continuing to study this compound in an effort to find an effective way to control it. Switching to the less polarizable F substituent should result in the formation of more advantageous O—H···O interactions. Despite the fact that interactions with F are usually considered to be weak, the O—H···F interactions seems to play a vital role in directing the molecular assembly of (II). The difference density map derived from the TAAM refinement shows polarizability of electron density around the F atom, which results in decreased repulsion between two neighbouring F atoms and, consequently, their closer distance.

This work was supported by the Narodowe Centrum Nauki (National Science Centre) in the framework of project DEC-2011/03/B/ST5/02755. KNJ thanks the Foundation for Polish Science for financial support within the START program. All authors thank the Interdisciplinary Centre for Mathematical and Computational Modelling in Warsaw (G33-14) and Wrocław Centre for Networking and Supercomputing (grant No. 285) for providing computational facilities. The support by Aldrich Chemical Co., Milwaukee, WI, USA, through continuous donation of chemicals and equipment is also gratefully acknowledged. We thank Dr Sian T. Howard for reading and correcting the manuscript.

References

Aakeröy, C. B., Fasulo, M., Schultheiss, N., Desper, J. & Moore, C. (2007). *J. Am. Chem. Soc.* **129**, 13772–13773.
Abramov, Yu. A. (1997). *Acta Cryst.* A**53**, 264–272.
Agilent (2011). *CrysAlisPro*. Agilent Technologies, Yarnton, England.
Allen, F. H. (2002). *Acta Cryst.* B**58**, 380–388.

Awwadi, F. F., Willett, R. D., Peterson, K. A. & Twamley, B. (2006). *Chem. Eur. J.* **12**, 8952–8960.

Bach, A., Lentz, D. & Luger, P. (2001). *J. Phys. Chem. A*, **105**, 7405–7412.

Bader, R. F. W. (1990). *Atoms in Molecules. A Quantum Theory*. Oxford: Clarendon Press.

Bąk, J. M., Dominiak, P. M., Wilson, C. C. & Woźniak, K. (2009). *Acta Cryst.* A**65**, 490–500.

Becke, A. D. (1988). *Phys. Rev. A*, **38**, 3098–3100.

Berger, R., Resnati, G., Metrangolo, P., Weber, E. & Hulliger, J. (2011). *Chem. Soc. Rev.* **40**, 3496–3508.

Biegler-König, F., Schönbohm, J. & Bayles, D. J. (2001). *J. Comput. Chem.* **22**, 545–559.

Blanco, F., Alkorta, I., Solimannejad, M. & Elguero, J. (2009). *J. Phys. Chem. A*, **113**, 3237–3244.

Blessing, R. H. (1995). *Acta Cryst.* A**51**, 33–38.

Blessing, R. H. (1997). *J. Appl. Cryst.* **30**, 421–426.

Bondi, A. (1964). *J. Phys. Chem.* **68**, 441–451.

Borowska, E., Durka, K., Luliński, S., Serwatowski, J. & Woźniak, K. (2012). *Eur. J. Org. Chem.* pp. 2208–2218.

Boys, S. F. & Bernardi, F. (1970). *Mol. Phys.* **19**, 553–566.

Bruker (2011). *APEX2, SAINT* and *SHELXTL*. Bruker AXS Inc., Madison, Wisconsin, USA.

Bui, T. T. T., Dahaoui, S., Lecomte, C., Desiraju, G. R. & Espinosa, E. (2009). *Angew. Chem. Int. Ed.* **48**, 3838–3841.

Chai, J., Wang, C., Jia, L., Pang, Y., Graham, M. & Cheng, S. Z. D. (2009). *Synth. Met.* **159**, 1443–1449.

Chen, J., Kampf, J. W. & Ashe, A. J. (2008). *Organometallics*, **27**, 3639–3641.

Chopra, D. (2012). *Cryst. Growth Des.* **12**, 541–546.

Chopra, D., Nagarajan, K. & Guru Row, T. N. (2005). *Cryst. Growth Des.* **5**, 1035–1039.

Cimino, P., Pavone, M. & Barone, V. (2007). *J. Phys. Chem. A*, **111**, 8482–8490.

Civalleri, B., Zicovich-Wilson, C. M., Valenzano, L. & Ugliengo, P. (2008). *CrystEngComm*, **10**, 405–410.

Collas, A., Borger, R. D., Amanova, T. & Blockhuys, F. (2010). *CrystEngComm*, **13**, 702–710.

Corradi, E., Meille, S. V., Messina, M. T., Metrangolo, P. & Resnati, G. (2000). *Angew. Chem. Int. Ed.* **39**, 1782–1786.

De Moliner, E., Brown, N. R. & Johnson, L. N. (2003). *Eur. J. Biochem.* **270**, 3174–3181.

Dikundwar, A. G. & Row, T. N. G. (2012). *Cryst. Growth Des.* **12**, 1713–1716.

Dittrich, B., Hübschle, C. B., Holstein, J. J. & Fabbiani, F. P. A. (2009). *J. Appl. Cryst.* **42**, 1110–1121.

Dittrich, B., Koritsánszky, T., Grosche, M., Scherer, W., Flaig, R., Wagner, A., Krane, H. G., Kessler, H., Riemer, C., Schreurs, A. M. M. & Luger, P. (2002). *Acta Cryst.* B**58**, 721–727.

Dovesi, R., Orlando, R., Civalleri, B., Roetti, R., Saunders, V. R. & Zicovich-Wilson, C. M. Z. (2005). *Z. Kristallogr.* **220**, 571–573.

Dovesi, R., Saunders, V. R., Roetti, R., Orlando, R., Zicovich-Wilson, C. M., Pascale, F., Civalleri, B., Doll, K., Harrison, N. M., Bush, I. J., D'Arco, P. & Llunell, M. (2009). *CRYSTAL09*. University of Torino, Italy.

Dunning, T. H. (1989). *J. Chem. Phys.* **90**, 1007–1023.

Durka, K., Jarzembska, K. N., Kamiński, R., Luliński, S., Serwatowski, J. & Woźniak, K. (2012). *Cryst. Growth Des.* **12**, 3720–3734.

Eskandari, K. & Zariny, H. (2010). *Chem. Phys. Lett.* **492**, 9–13.

Espinosa, E., Lecomte, C. & Molins, E. (1999). *Chem. Phys. Lett.* **300**, 745–748.

Espinosa, E., Molins, E. & Lecomte, C. (1998). *Chem. Phys. Lett.* **285**, 170–173.

Faerman, C. H. & Price, S. L. (1990). *J. Am. Chem. Soc.* **112**, 4915–4926.

Farrugia, L. J. (2012). *J. Appl. Cryst.* **45**, 849–854.

Feyereisen, M. W., Feller, D. & Dixon, D. A. (1996). *J. Phys. Chem.* **100**, 2993–2997.

Frisch, M. J. *et al.* (2009). *GAUSSIAN09*. Gaussian Inc., Pittsburgh, Pennsylvania, USA.

Fu, Y. & Brock, C. P. (1998). *Acta Cryst.* B**54**, 308–315.

Gavezzotti, A. (2002). *J. Phys. Chem. B*, **106**, 4145–4154.

Gavezzotti, A. (2003*a*). *J. Phys. Chem. B*, **107**, 2344–2353.

Gavezzotti, A. (2003*b*). *CrystEngComm*, **5**, 429–438.

Gilli, P. & Gilli, G. (2009). *The Nature of the Hydrogen Bond*. New York: Oxford University Press.

Grabowski, S. J. (2006). *Hydrogen Bonding: New Insights*. Dordrecht: Springer.

Grimme, S. (2004). *J. Comput. Chem.* **25**, 1463–1473.

Grimme, S. (2006). *J. Comput. Chem.* **27**, 1787–1799.

Gu, Y., Kar, T. & Scheiner, S. (1999). *J. Am. Chem. Soc.* **121**, 9411–9422.

Hall, D. G. (2005). *Boronic Acids*. Weinheim: Wiley-VCH.

Hansen, N. K. & Coppens, P. (1978). *Acta Cryst.* A**34**, 909–921.

Hassel, O. (1970). *Science*, **170**, 497–502.

Hathwar, V. R., Gonnade, R. G., Munshi, P., Bhadbhade, M. M. & Guru Row, T. N. (2011). *Cryst. Growth Des.* **11**, 1855–1862.

Hathwar, V. R. & Row, T. N. G. (2011). *Cryst. Growth Des.* **11**, 1338–1346.

Hathwar, V. R., Thakur, T. S., Dubey, R., Pavan, M. S., Row, T. N. G. & Desiraju, G. R. (2011). *J. Phys. Chem. A*, **115**, 12852–12863.

Januszewski, E., Lorbach, A., Grewal, R., Bolte, M., Bats, J. W., Lerner, H. W. & Wagner, M. (2011). *Chem. Eur. J.* **17**, 12696–12705.

Jarzembska, K. N. & Dominiak, P. M. (2012). *Acta Cryst.* A**68**, 139–147.

Jarzembska, K. N., Goral, A. M., Gajda, R. & Dominiak, P. M. (2013). *Cryst. Growth Des.* **13**, 239–254.

Jarzembska, K. N., Kamiński, R., Wenger, E., Lecomte, C. & Dominiak, P. M. (2013). *J. Phys. Chem. C*, **117**, 7764–7775.

Jarzembska, K. N., Kubsik, M., Kamiński, R., Woźniak, K. & Dominiak, P. M. (2012). *Cryst. Growth Des.* **12**, 2508–2524.

Jeffrey, G. A. (1997). *An Introduction to Hydrogen Bonding*. New York: Oxford University Press.

Jelsch, C., Guillot, B., Lagoutte, A. & Lecomte, C. (2005). *J. Appl. Cryst.* **38**, 38–54.

Kessler, S. N., Neuburger, M. & Wegner, H. A. (2011). *Eur. J. Org. Chem.* pp. 3238–3245.

Kessler, S. N. & Wegner, H. A. (2010). *Org. Lett.* **12**, 4062–4065.

Kirsop, P., Storey, J. M. D. & Harrison, W. T. A. (2004). *Acta Cryst.* C**60**, o353–o355.

Krishnan, R., Binkley, J. S., Seeger, R. & Pople, J. A. (1980). *J. Chem. Phys.* **72**, 650–654.

Lee, C., Yang, W. & Parr, R. G. (1988). *Phys. Rev. B*, **37**, 785–789.

Lu, Y., Zou, J., Yu, Q., Jiang, Y. & Zhao, W. (2007). *Chem. Phys. Lett.* **449**, 6–10.

Luliński, S., Smętek, J., Durka, K. & Serwatowski, J. (2013). *Eur. J. Org. Chem.* pp. 8315–8322.

Mariaca, R., Behrnd, N.-R., Eggli, P., Stoeckli-Evans, H. & Hulliger, J. (2006). *CrystEngComm*, **8**, 222–232.

Maschio, L., Civalleri, B., Ugliengo, P. & Gavezzotti, A. (2011). *J. Phys. Chem. A*, **115**, 11179–11186.

Matta, C. F. & Boyd, R. J. (2007). *The Quantum Theory of Atoms in Molecules: From Solid State to DNA and Drug Design*. Weinheim: Wiley-VCH.

McKinnon, J. J., Mitchell, A. S. & Spackman, M. A. (1998). *Chem. Eur. J.* **4**, 2136–2141.

McKinnon, J. J., Spackman, M. A. & Mitchell, A. S. (2004). *Acta Cryst.* B**60**, 627–668.

Metrangolo, P., Murray, J. S., Pilati, T., Politzer, P., Resnati, G. & Terraneo, G. (2011). *Cryst. Growth Des.* **11**, 4238–4246.

Metrangolo, P. & Resnati, G. (2008*a*). *Halogen-Bonding: Fundamentals and Applications*. Berlin: Springer.

Metrangolo, P. & Resnati, G. (2008*b*). *Science*, **321**, 918–919.

Metrangolo, P. & Resnati, G. (2012). *Cryst. Growth Des.* **12**, 5835–5838.

Metz, M. V., Schwartz, D. J., Stern, C. L., Nickias, P. N. & Marks, T. J. (2000). *Angew. Chem. Int. Ed.* **112**, 1368–1372.
Møller, C. & Plesset, M. S. (1934). *Pure Appl. Chem.* **46**, 618–622.
Mugnaini, V., Punta, C., Liantonio, R., Metrangolo, P., Recupero, F., Resnati, G., Pedulli, G. F. & Lucarini, M. (2006). *Tetrahedron Lett.* **47**, 3265–3269.
Murray, J. S., Lane, P. & Politzer, P. (2009). *J. Mol. Model.* **15**, 723–729.
Nayak, S. K., Reddy, M. K., Guru Row, T. N. & Chopra, D. (2011). *Cryst. Growth Des.* **11**, 1578–1596.
Oswald, I. D. H., Allan, D. R., Day, G. M., Motherwell, W. D. S. & Parsons, S. (2005). *Cryst. Growth Des.* **5**, 1055–1071.
Oswald, I. D. H., Allan, D. R., Motherwell, W. D. S. & Parsons, S. (2005). *Acta Cryst.* B**61**, 69–79.
Pedireddi, V. R., Reddy, D. S., Goud, B. S., Craig, D. C., Rae, A. D. & Desiraju, G. R. (1994). *J. Chem. Soc. Perkin Trans. 2*, pp. 2353–2360.
Perdew, J. (1986). *Phys. Rev. B*, **33**, 8822–8824.
Politzer, P., Murray, J. S. & Concha, M. C. (2008). *J. Mol. Model.* **14**, 659–665.
Ponomarev, V. I. & Shilov, G. V. (1983). *Z. Kristallogr.* **28**, 674–677.
Popelier, P. L. A. (2000). *Atoms in Molecules, an Introduction.* New York: Prentice Hall.
Priimagi, A., Cavallo, G., Forni, A., Gorynsztejn-Leben, M., Kaivola, M., Metrangolo, P., Milani, R., Shishido, A., Pilati, T. & Resnati, G. (2012). *Adv. Funct. Mater.* **22**, 2572–2579.
Ramasubbu, N., Parthasarathy, R. & Murray-Rust, P. (1986). *J. Am. Chem. Soc.* **108**, 4308–4314.
Reichenbächer, K., Süss, H. I., Stoeckli-Evans, H., Bracco, S., Sozzani, P., Weber, E. & Hulliger, J. (2004). *New J. Chem.* **28**, 393–397.
Schwarzer, A., Seichter, W., Weber, E., Stoeckli-Evans, H., Losada, M. & Hulliger, J. (2004). *CrystEngComm*, **6**, 567–572.
Schwarzer, A. & Weber, E. (2008). *Cryst. Growth Des.* **8**, 2862–2874.
Sheldrick, G. M. (2008). *Acta Cryst.* A**64**, 112–122.
Sluis, P. van der & Spek, A. L. (1990). *Acta Cryst.* A**46**, 194–201.
Spackman, M. A. & Byrom, P. G. (1997). *Chem. Phys. Lett.* **267**, 215–220.
Spek, A. L. (2009). *Acta Cryst.* D**65**, 148–155.
Stammler, H., Vishnevskiy, Y. V., Sicking, C. & Mitzel, N. W. (2013). *CrystEngComm*, **15**, 3536–3546.
Takemura, H., Ueda, R. & Iwanaga, T. (2009). *J. Fluorine Chem.* **130**, 684–688.
Turner, M. J., McKinnon, J. J., Jayatilaka, D. & Spackman, M. A. (2011). *CrystEngComm*, **13**, 1804–1813.
Volkov, A., Li, X., Koritsanszky, T. & Coppens, P. (2004). *J. Phys. Chem. A*, **108**, 4283–4300.
Volkov, A., Messerschmidt, M. & Coppens, P. (2007). *Acta Cryst.* D**63**, 160–170.
Xu, L., Zou, J.-W., Lu, Y.-X., Yu, Q.-S. & Zhang, N. (2009). *Comput. Theor. Chem.* **897**, 12–16.